Supporting information

Ionic Liquid-Stabilized Vanadium Oxo-clusters Catalyzing Alkane Oxidation by Regulating Oligovanadates

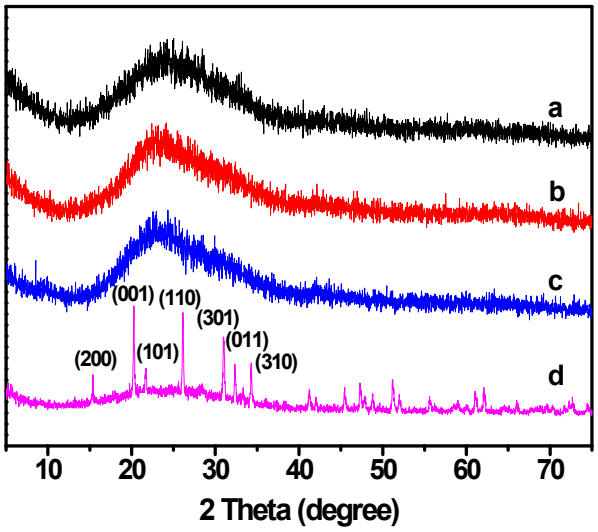

Figure S1. XRD patterns of IL [TBA][Pic]-stabilized V oxo-clusters. a) V-OC@IL-0.5, b) V-OC@IL-1, c) V-OC@IL-2, d) Commercial V_2O_5.

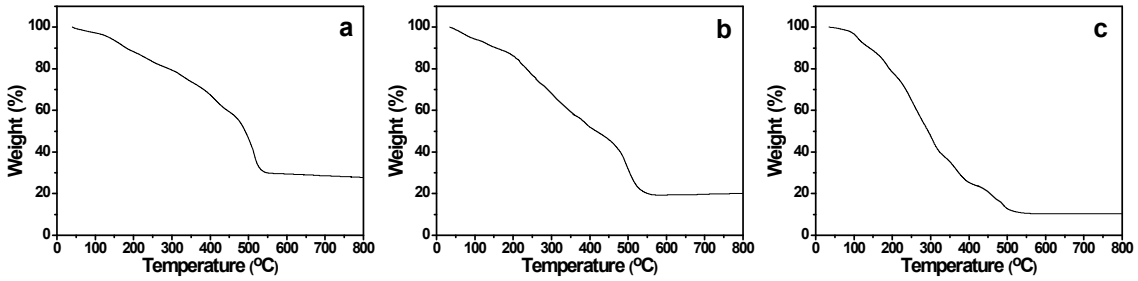

Figure S2. TGA patterns of IL [TBA][Pic]-stabilized V oxo-clusters. a) V-OC@IL-0.5, b) V-OC@IL-1, c) V-OC@IL-2.

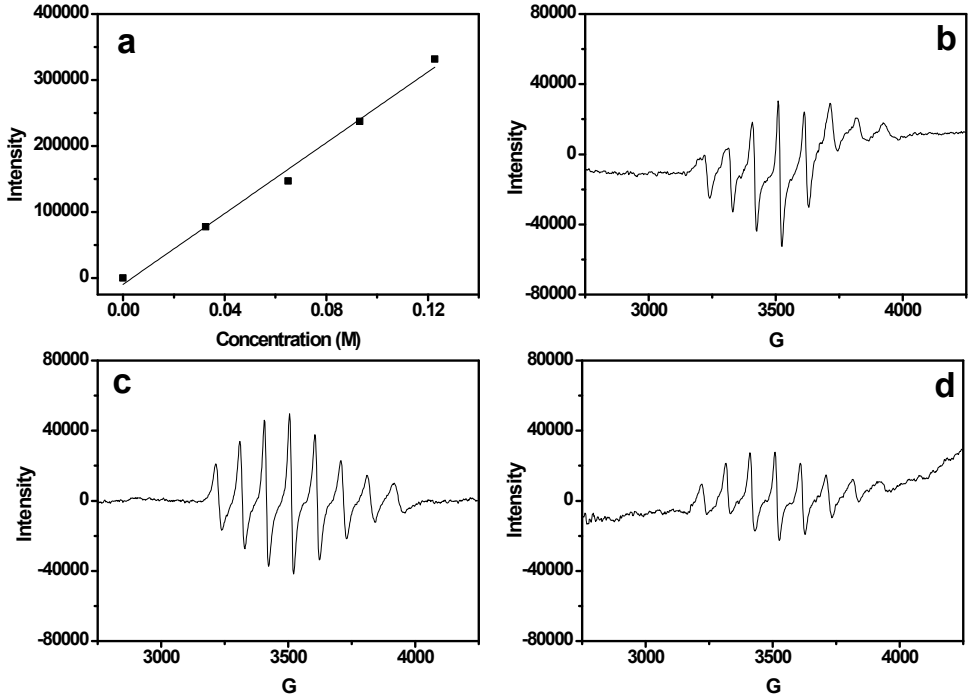

Figure S3. a) EPR signal intensity as a function of Vanadium (IV) concentration. The standard curve was achieved with the different concentrations (0.03 M–0.13 M) of $VOSO_4$ solution (V(IV)). b–d) EPR spectra of V-OC@IL-n (n=0.5,1,2) in H_2O at 298 K. The concentration of V (IV) in the oxo-cluster was quantified by external standard method.

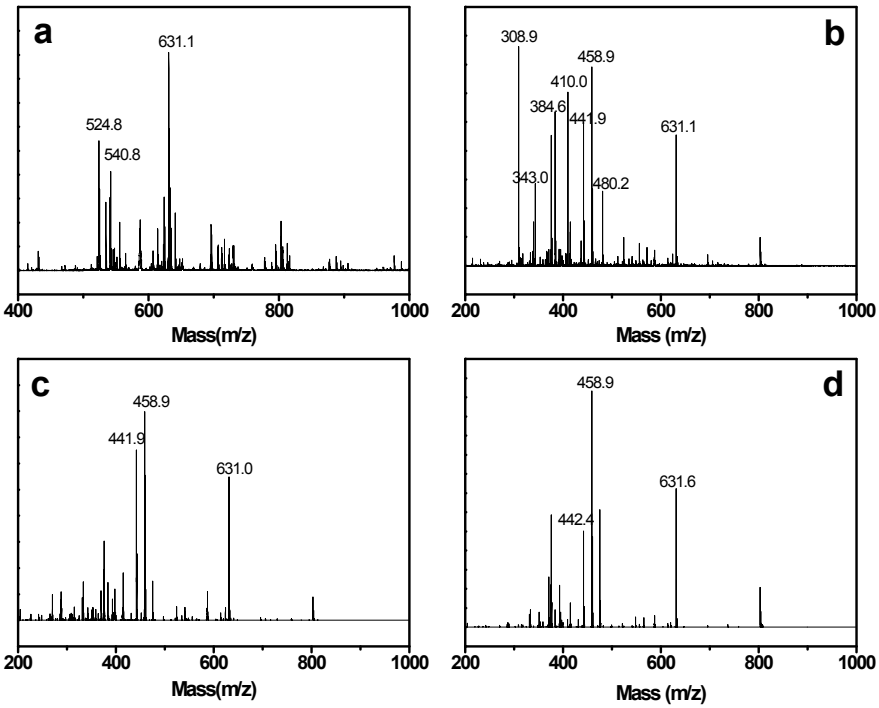

Figure S4. Mass spectra of the different catalysts. a) V-OC@IL-1; b) V-OC@IL-2; c) oxidizing species of V-OC@IL-1; d) The fresh solution was obtained by mixing V_2O_5 and IL [TBA][Pic] in the presence of H_2O_2 (molar ratio IL/V=1:1), and then subjected to MS characterization.

Table S1. Possible structures of V oxo-cluster V-OC@IL-n (n=1 and 2) and the oxidizing species of V-OC@IL-1

Entry	Mass (m/z)	Possible structure	
1	343.0	$[V(O)(O\text{-}O)(pic)_2]^-$	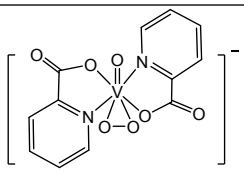
2	410.0	$[V_2(O)_3(\mu\text{-}O)(pic)_2]^-$	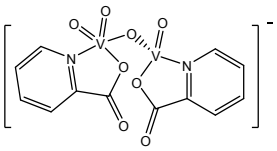
3	524.8	$[V_3(O)_2(O\text{-}O)_2(\mu\text{-}O)_2(pic)_2]^-$	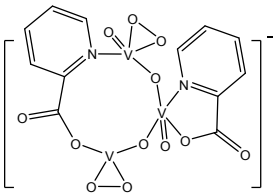
4	540.8	$[V_3(O)(O\text{-}O)_3(\mu\text{-}O)_2(pic)_2]^-$	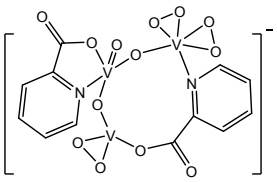
5	631.1	$[V_3(O)_3(O\text{-}O)(\mu\text{-}O)_2(pic)_3]^-$	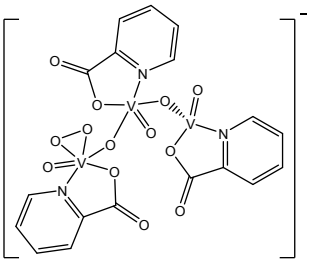
6	441.9	$[V_2(O)_2(O\text{-}O)\ (OH)(\mu\text{-}O)(pic)_2]^-$ $[M\text{-}H]^-$	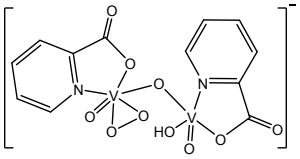
7	458.9	$[V_2(O)(O\text{-}O)_2(OH)(\mu\text{-}O)(pic)_2]^-$	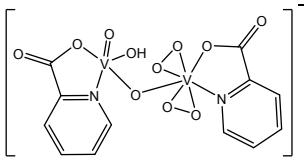

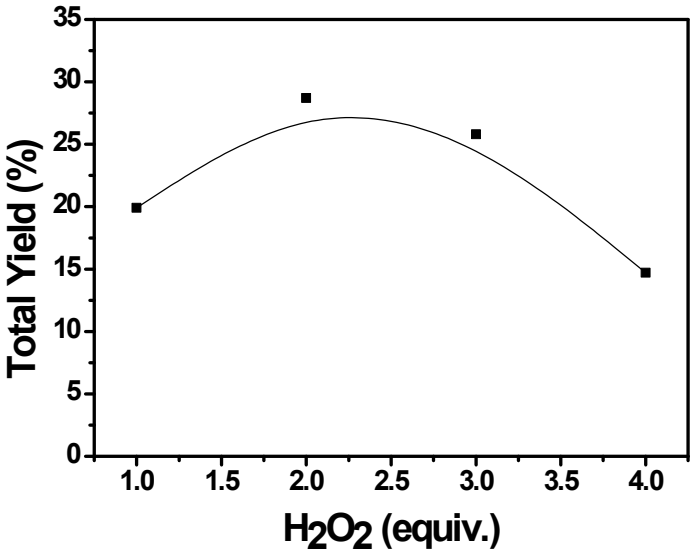

Figure S5. The effect of initial amount of H_2O_2 on cyclohexane oxidation. Reaction conditions: cyclohexane (5.0 mmol), H_2O_2 (30% aqueous solution), V-OC@IL-1 (10 mg), CH_3CN (3.0 mL), 50 °C, 1 h.

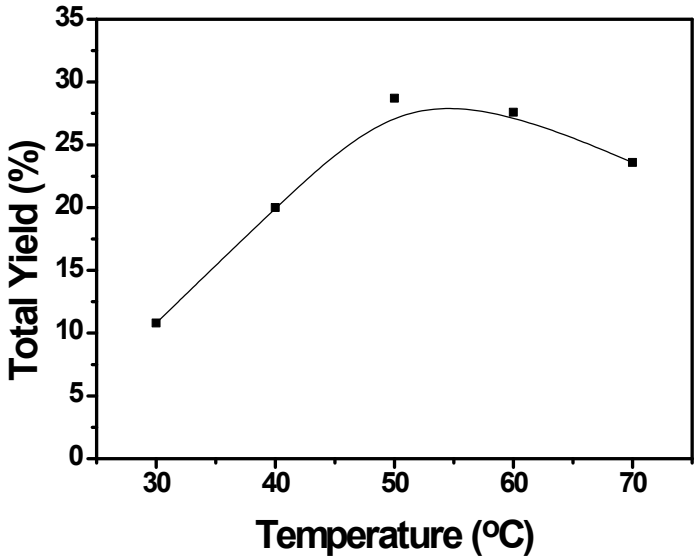

Figure S6. The effect of reaction temperature on cyclohexane oxidation. Reaction conditions: cyclohexane (5.0 mmol), H_2O_2 (10.0 mmol, 30% aqueous solution), V-OC@IL-1 (10 mg), CH_3CN (3.0 mL), 1 h.

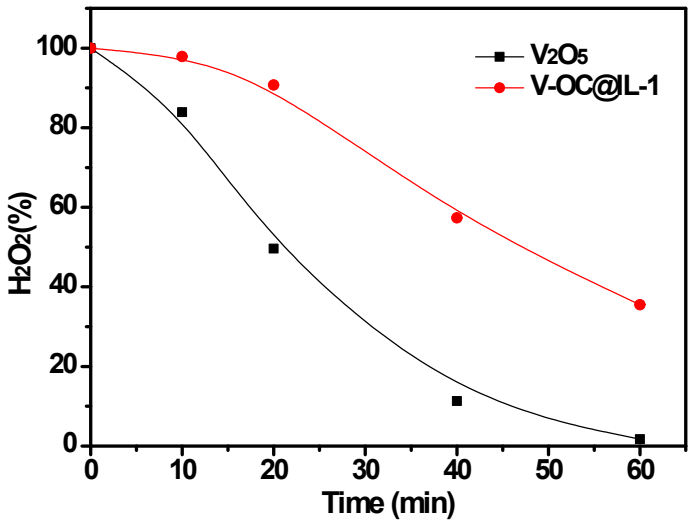

Figure S7. Hydrogen peroxide degradation curves over V_2O_5 and V-OC@IL-1. Reaction conditions: H_2O_2 (10.0 mmol, 30% aqueous solution), catalyst (0.1 mmol V), CH_3CN (3.0 mL), 50 °C.

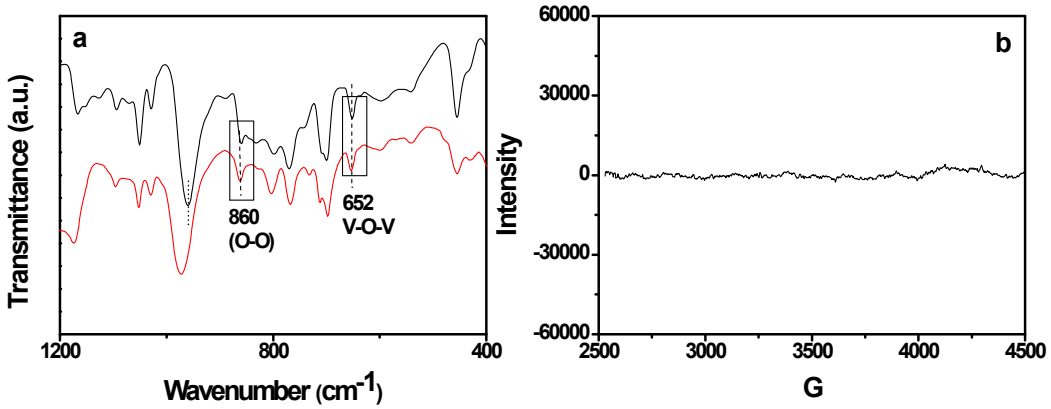

Figure S8. a) FT-IR spectra of V-OC@IL-1 (top) and its oxidizing species (bottom); b) EPR spectrum of the oxidizing species of V-OC@IL-1.

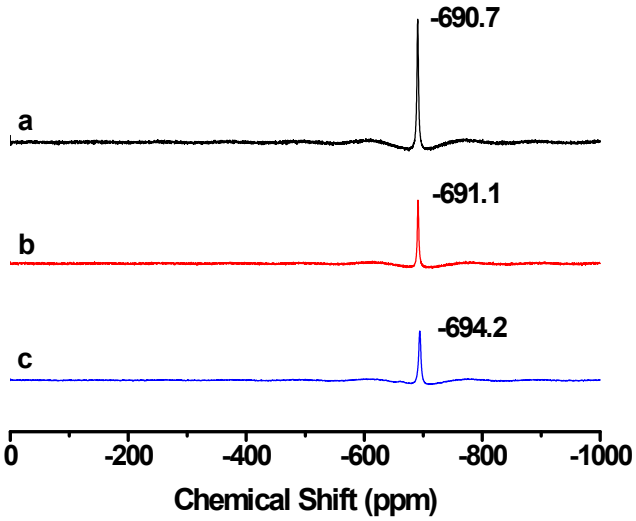

Figure S9. ^{51}V NMR spectra of vanadium species prepared from V_2O_5 under the action of H_2O_2 in the presence of ionic liquid: a) [TBA][OAc], b) [BMIM][OAc] and c) [BMIM][BF_4], respectively.

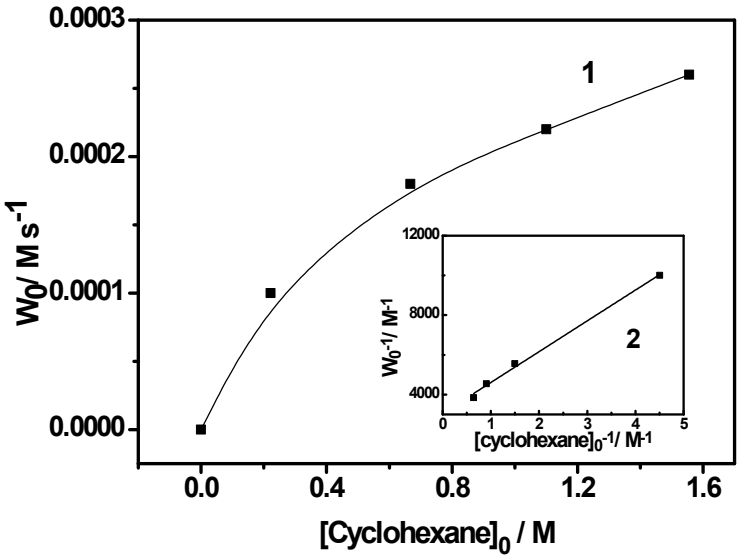

Figure S10. Oxidation of cyclohexane with hydrogen peroxide (2.22 M, 30 % aqueous solution) catalyzed by V-OC@IL-1 (0.004 M) in CH_3CN at 50 °C (the total initial content of water in the reaction mixture was constant = 9.7 M). Dependence of the initial rate of oxygenate formation, W_0, on the initial concentration of cyclohexane is shown (curve 1). Linearization of curve 1 in coordinates $[cyclohexane]_0^{-1}$, W_0 is presented in line 2. Concentrations of cyclohexanone and cyclohexanol were determined after reduction of the aliquots with solid PPh_3.

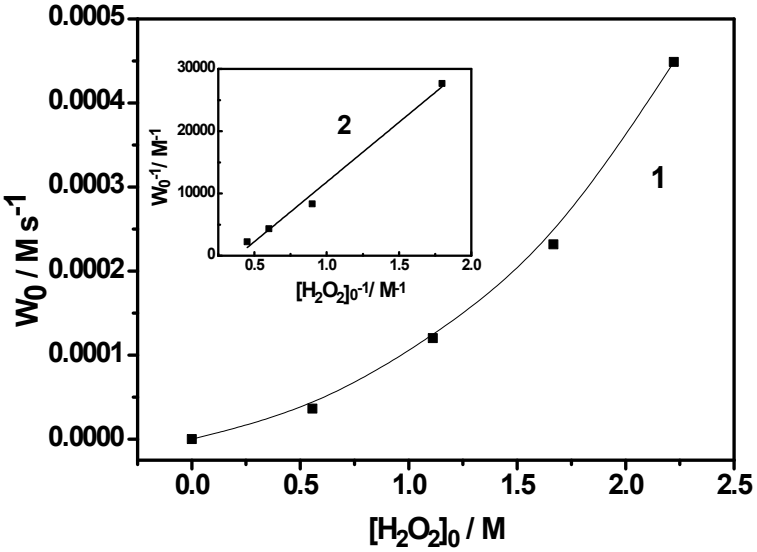

Figure S11. Oxidation of cyclohexane (1.11 M) with hydrogen peroxide (30 % aqueous solution) catalyzed by V-OC@IL-1 (0.004 M) in CH_3CN at 50 °C (the total initial content of water in the reaction mixture was constant = 9.7 M). Dependence of the initial rate of oxygenate formation, W_0, on the initial concentration of H_2O_2 is shown (curve 1). Linearization of curve 1 in coordinates $[H_2O_2]_0^{-1}$, W_0 is presented in line 2. Concentrations of cyclohexanone and cyclohexanol were determined after reduction of the aliquots with solid PPh_3.

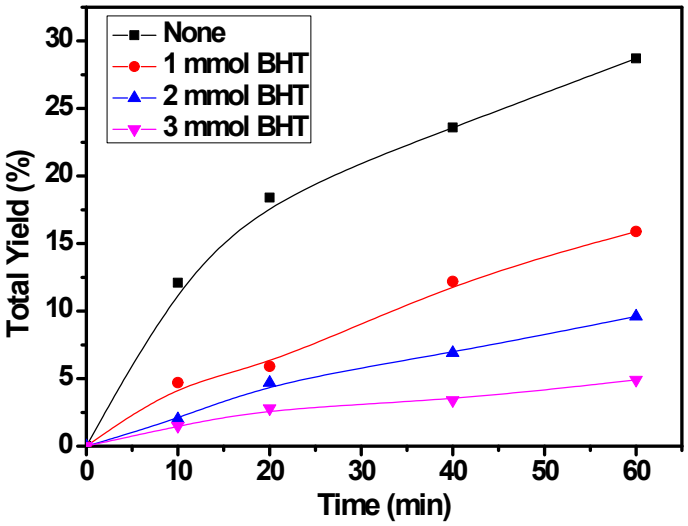

Figure S12. The effect of butylated hydroxytoluene (BHT) amount on the oxidation of cyclohexane. Reaction conditions: cyclohexane (5.0 mmol), H_2O_2 (10.0 mmol, 30% aqueous solution), V-OC@IL-1(0.4 mol%), CH_3CN (3.0 mL), 50 °C.

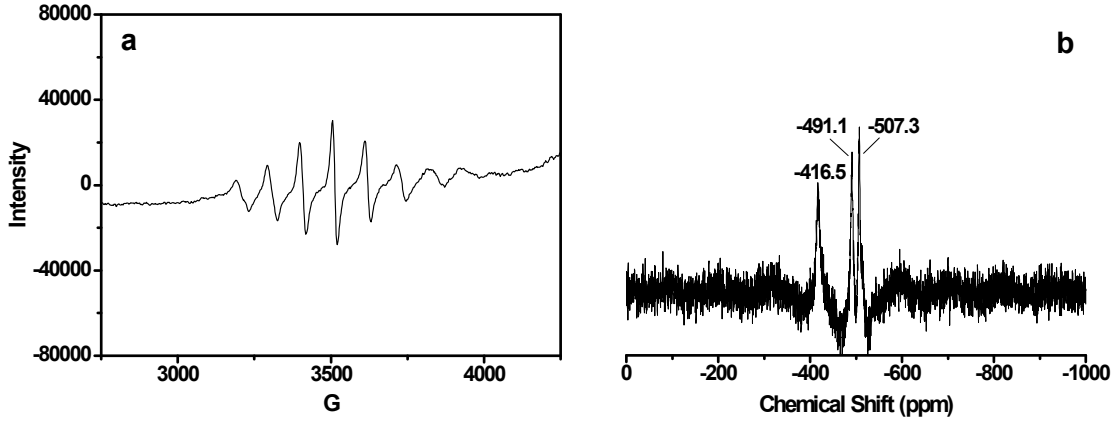

Figure S13. EPR spectrum (a) and ^{51}V NMR spectrum (b) of the recovered V-OC@IL-1 catalyst.

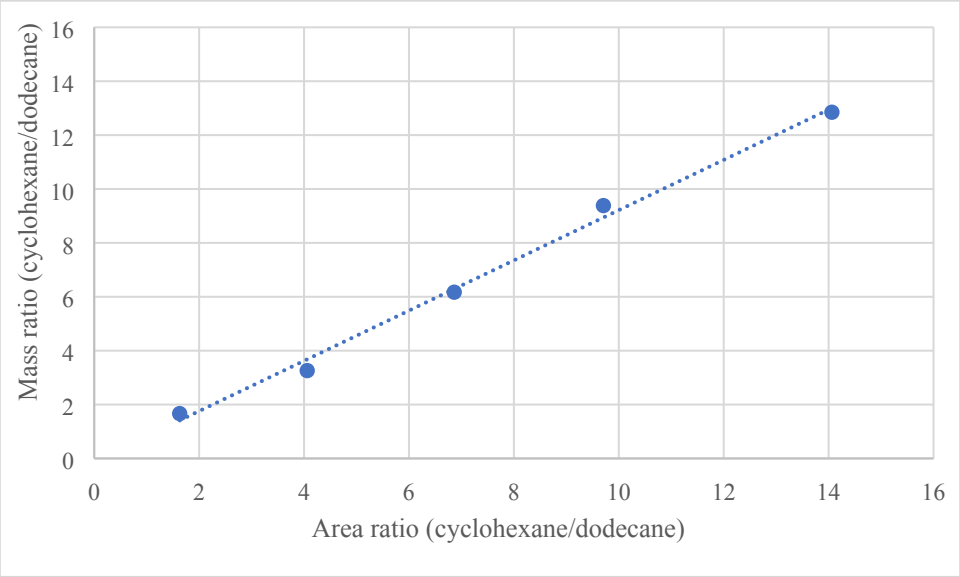

Figure S14. GC calibration line for cyclohexane with dodecane as internal standard.

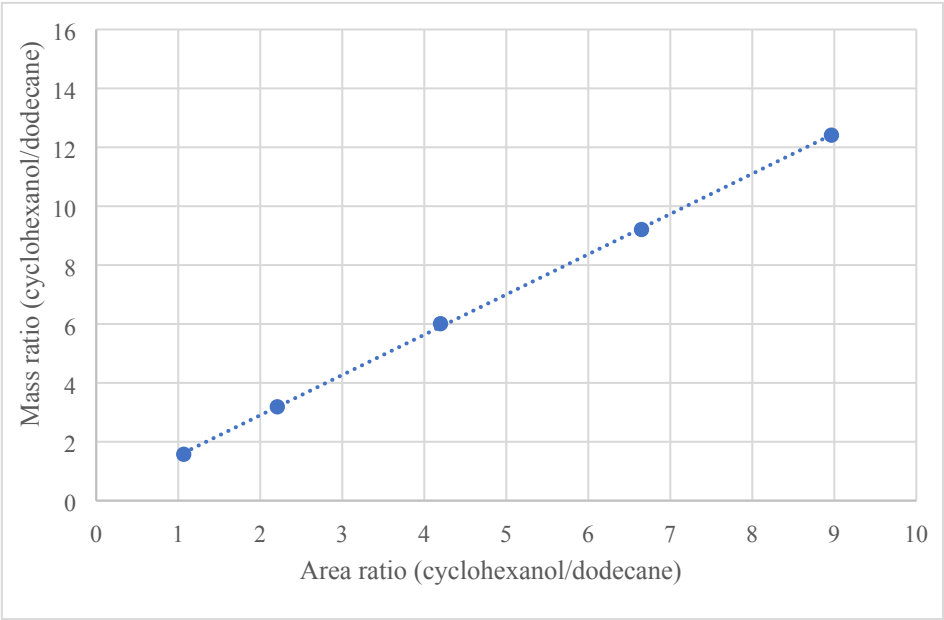

Figure S15. GC calibration line for cyclohexanol with dodecane as internal standard.

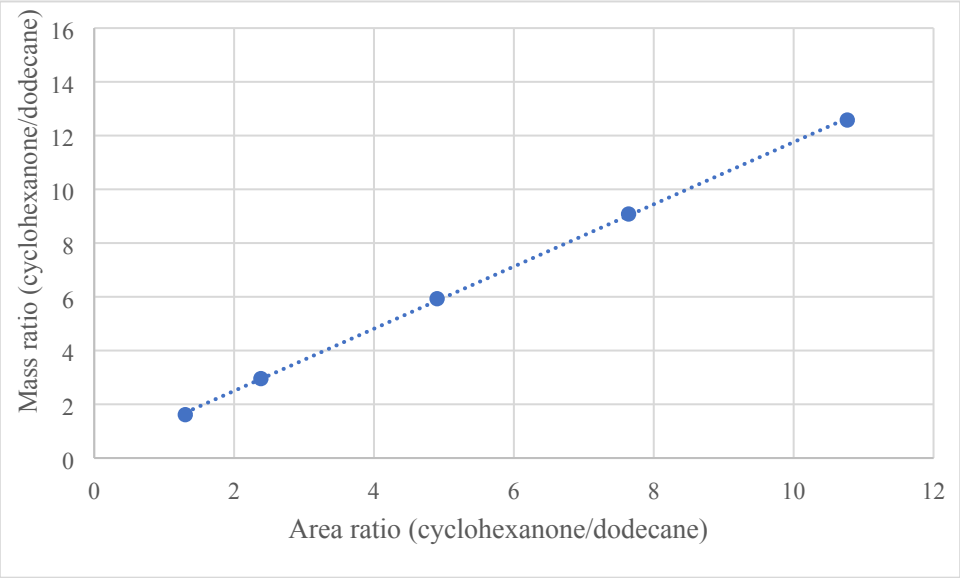

Figure S16. GC calibration line for cyclohexanone with dodecane as internal standard.

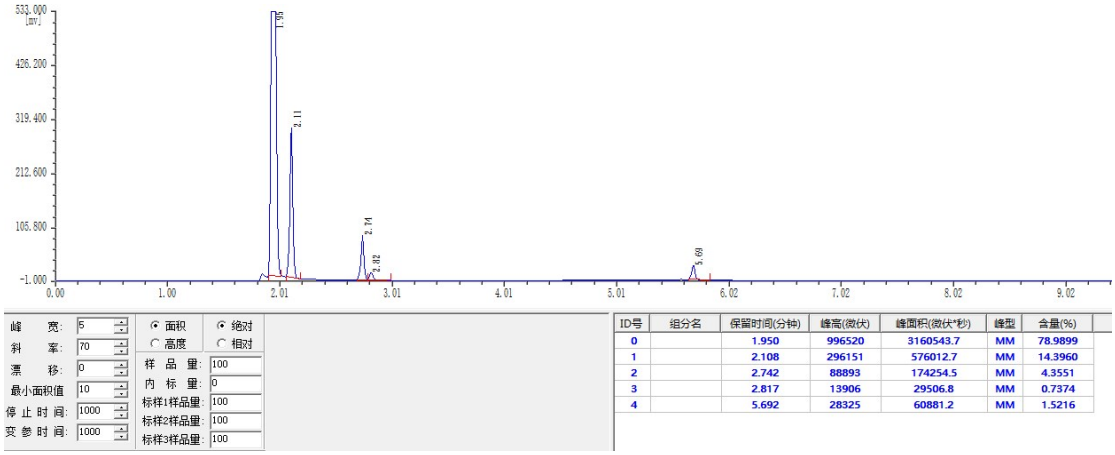

Figure S17. Chromatogram example of reaction solution. The cyclohexane and the products are identified as follows (retention times in parentheses): cyclohexane (2.11 min), cyclohexanol (2.74 min), cyclohexanone (2.82 min), dodecane (internal standard, 5.69 min).

Table S2. Comparison of the V-OC@IL-1 catalyst with those reported catalytic systems in the selective oxidation of cyclohexane.

Catalysts	Reaction conditions	Yield of KA oil (%)	Ref.
None or Co complex (industrial production)	160–170 °C, air	<5	S1
$[\{Cu(Hdea)(H_2dea)\}_2(\mu_2\text{-}H_2pma)]\cdot 3H_2O$	50 °C, 5 h, H_2O_2, n(H_2O_2)/ n(cyclohexane) = 5	33.5	S2
$[Cu(\kappa ONN'\text{-}HL)(NO_3)(DMF)](NO_3)\cdot H_2$	50 °C, 3 h, H_2O_2, pyridine, n(H_2O_2)/ n(cyclohexane) = 5	21.6	S3
$[VO(OCH_3)(5\text{-Cl-quin})_2]$	50 °C, 1 h, H_2O_2, n(H_2O_2)/ n(cyclohexane) = 4.3	39	S4
CuSBdiAP	70 °C, 3 h, H_2O_2, n(H_2O_2)/ n(cyclohexane) = 1.5	27.68	S5
CeCr/NC-500	60 °C, 5 h, H_2O_2, n(H_2O_2)/ n(cyclohexane) = 2	53.9	S6
Cl-PCFe	150 °C, 2 h, 1.0 MPa O_2	12.1	S7
Co-MgAlO	150 °C, 2 h, 0.6 MPa O_2	7.5	S8
AC	125 °C, 8 h, 1.5 MPa O_2	5.3	S9
$C_6MHImHSO_4$-Co/ZSM-5	150 °C, 3 h, 1.5 MPa air	8.9	S10
V-OC@IL-1	50 °C, 1 h, H_2O_2, n(H_2O_2)/ n(cyclohexane) = 2	28.7	This work

References

S1 X. Liu, M. Conte, Q. He, D. W. Knight, D. M. Murphy, S. H. Taylor, K. Whiston, C. J. Kiely and G. J. Hutchings, *Chem. - Eur. J.*, 2017, **23**, 11834–11842.

S2 T. A. Fernandes, C. I. M. Santos, V. André, S. S. P. Dias, M. V. Kirillova and A. M. Kirillov, *Catal. Sci. Technol.*, 2016, **6**, 4584–4593.

S3 O. V. Nesterova, D. S. Nesterov, A. Krogul-Sobczak, M. F. C. G. da Silva and A. J. L. Pombeiro, *J. Mol. Catal. A: Chem.*, 2017, **426**, 506–515.

S4 I. Gryca, K. Czerwińska, B. Machura, A. Chrobok, L. S. Shul'pina, M. L. Kuznetsov, D. S. Nesterov, Y. N. Kozlov, A. J. L. Pombeiro, I. A. Varyan and G. B. Shul'pin, *Inorg. Chem.*, 2018, **57**, 1824−1839.

S5 A. A. Alshaheri, M. I. M. Tahir, M. B. A. Rahman, T. B. S. A. Ravoof and T. A. Saleh, *Chem. Eng. J.*, 2017, **327**, 423–430.

S6 C. Xu, L. L. Jin, X. Z. Wang, Y. Q. Chen and L. Y. Dai, *Carbon*, 2020, **160**, 287−297.

S7 S. T. Wu, Y. R. He, C. H. Wang, C. M. Zhu, J. Shi, Z. Y. Chen, Y. Wan, F. Hao, W. Xiong, P. L. Liu and H. A. Luo, *ACS Appl. Mater. Interfaces*, 2020, **12**, 26733−26745.

S8 P. Liu, K. Y. You, R. J. Deng, Z. P. Chen, J. Jian, F. F. Zhao, P. L. Liu, Q. H. Ai and H. A. Luo, *Mol. Catal.*, 2019, **466**, 130−137.

S9 Y. Guo, T. Ying, X. H. Liu, B. F. Shi and Y. Q. Wang, *Mol. Catal.*, 2019, **479**, 110487−110493.

S10 Y. Hong, Y. X. Fang, X. T. Zhou, G. Du, J. J. Mai, D. L. Sun and Z. P. Shao, *Ind. Eng. Chem. Res.*, 2019, **58**, 19832−19838.